Clim Dyn (2015) 44:279–297
DOI 10.1007/s00382-014-2260-z

Response of the North African summer monsoon to precession and obliquity forcings in the EC-Earth GCM

J. H. C. Bosmans · S. S. Drijfhout · E. Tuenter · F. J. Hilgen · L. J. Lourens

Received: 10 June 2013 / Accepted: 11 July 2014 / Published online: 1 August 2014

Abstract We investigate, for the first time, the response of the North African summer monsoon to separate precession and obliquity forcings using a high-resolution state-of-the-art coupled general circulation model, EC-Earth. Our aim is to better understand the mechanisms underlying the astronomical forcing of this low-latitude climate system in detail. The North African monsoon is strengthened when northern hemisphere summer insolation is higher, as is the case in the minimum precession and maximum obliquity experiments. In these experiments, the low surface pressure areas over the Sahara are intensified and located farther north, and the meridional pressure gradient is further enhanced by a stronger South Atlantic high pressure area. As a result, the southwesterly monsoon winds are stronger and bring more moisture into the monsoon region from both the northern and southern tropical Atlantic. The monsoon winds, precipitation and convection also extend farther north into North Africa. The precession-induced changes are much larger than those induced by obliquity, but the latter are remarkable because obliquity-induced changes in summer insolation over the tropics are nearly zero. Our results provide a different explanation than previously proposed for mechanisms underlying the precession- and, especially, obliquity-related signals in paleoclimate proxy records of the North African monsoon. The EC-Earth experiments reveal that, instead of higher latitude mechanisms, increased moisture transport from both the northern and southern tropical Atlantic is responsible for the precession and obliquity signals in the North African monsoon. This increased moisture transport results from both increased insolation and an increased tropical insolation gradient.

Keywords Paleoclimate modelling · Astronomical forcing · Milankovitch cycles · North African monsoon

J. H. C. Bosmans · E. Tuenter · F. J. Hilgen · L. J. Lourens
Department of Earth Sciences, Faculty of Geosciences, Utrecht University, Budapestlaan 4, 3584 CD Utrecht, The Netherlands

J. H. C. Bosmans · S. S. Drijfhout · E. Tuenter
Global Climate, Royal Netherlands Meteorological Institute (KNMI), P.O. Box 201, 3730 AE De Bilt, The Netherlands

Present Address:
J. H. C. Bosmans (✉)
Department of Physical Geography, Faculty of Geosciences, Utrecht University, Heidelberglaan 2, 3584 CS Utrecht, The Netherlands
e-mail: J.H.C.Bosmans@uu.nl

S. S. Drijfhout
National Oceanographic Centre, European Way, Southampton SO14 3ZH, UK

Present Address:
E. Tuenter
Royal Netherlands Meteorological Institute (KNMI), P.O. box 201, 3730 AE De Bilt, The Netherlands

1 Introduction

Sedimentary records from North Africa and its surrounding oceans suggest that the North African summer monsoon responds strongly to astronomical forcing (e.g. Rossignol-Strick 1985; Pokras and Mix 1987; Larrasoaña et al. 2003). Changes in monsoon intensity are mainly driven by the precessional cycle, which dominates the changes in incoming solar radiation (insolation) over the tropics. Precession is affected by eccentricity and has a strong effect on the seasonal cycle of the incoming solar radiation. Evidence for an obliquity (axial tilt) component has been found as well (Lourens et al. 1996, 2001), despite the near absence

of obliquity-induced summer insolation changes over the tropics.

Numerous climate modelling studies have confirmed the impact of astronomical cycles on the monsoon systems. Most of these modelling studies use time slices of the last glacials and interglacials, such as the Eemian (~126 ka, kyr before present) and glacial inception at 115 ka (e.g. Prell and Kutzbach 1987; de Noblet et al. 1996; Montoya et al. 2000; Braconnot et al. 2008), as well as the Last Glacial Maximum and the Holocene, including some of the earliest modelling studies (e.g. Kutzbach 1981) and many PMIP-simulations (e.g. Braconnot et al. 2007). In these modelling studies, the combined effect of all orbital parameters (eccentricity, precession and obliquity) on monsoon intensity are investigated. These studies agree that at times of increased northern hemisphere summer insolation, warming of the continents results in deeper thermal lows and increased ocean–land thermal and pressure gradients. As a result, monsoon winds and moisture transport from ocean to land are intensified and continental summer monsoon precipitation is enhanced. Furthermore, temperatures in the monsoon areas are reduced due to increased evaporation and cloud cover (e.g. de Noblet et al. 1996; Montoya et al. 2000; Braconnot et al. 2007).

At present, there are not many studies that examine the precession and obliquity signals in the North African summer monsoon separately. The few that do focus mainly on precession. Short and Mengel (1986) used an energy balance model (EBM) to investigate the response of the tropics to precession. Their study shows precession-driven changes in the temperature contrast between North Africa and the tropical Atlantic, which indicates changes in moisture availability to the monsoon area in the rainy season. Prell and Kutzbach (1987) performed idealized precession and obliquity experiments with an atmospheric general circulation model (AGCM) in permanent July mode. Their work agrees with the above-mentioned increase in the land–ocean pressure gradient, stronger monsoon winds and enhanced monsoon precipitation at times of increased northern hemisphere summer insolation. The precession effect on subtropical highs is investigated by Mantsis et al. (2013), who also identified increased convective precipitation over the monsoon areas. Merlis et al. (2013a, b) use idealized aqua-planet simulations to show that the hemisphere that receives most summer insolation also receives more precipitation, and that over an idealized subtropical continent the monsoon shifts polewards. The study of Erb et al. (2013) also identifies increased moisture transport into the monsoon areas as well as a poleward shift in monsoonal precipitation for both precession- and obliquity-induced increases in summer insolation. In their obliquity experiments Prell and Kutzbach (1987) and Erb et al. (2013) keep eccentricity and precession at their present-day values, which may affect the results since the obliquity-induced changes are sensitive to the prevailing precession (Tuenter et al. 2003).

The only study, to our knowledge, that has examined the separate precession and obliquity effects on the North African monsoon is that of Tuenter et al. (2003). Using an intermediate complexity quasi-geostrophic model, EC-Bilt, they investigated the climate response to the separate astronomical forcings. They found a stronger and more northward monsoon over North Africa at times of minimum precession or maximum obliquity, when summer insolation is increased. In addition they showed that insolation changes at high latitudes play an important role in both the precession and obliquity experiments. As a result of a stronger convergence zone over southern Asia due to enhanced summer insolation, stronger winds extend from the Atlantic, via North Africa, into Asia in the EC-Bilt model. Furthermore there is increased moisture transport from the north into the North African monsoon region. Such mechanisms can explain why obliquity affects the North African monsoon despite the near lack of summer insolation change over the tropics. Local precession-induced insolation changes over the tropics also play an important role, as insolation changes over the tropics are strong and induce a stronger land–sea contrast, which dominates the remote effects.

A weakness of the quasi-geostrophic model EC-Bilt is that it cannot capture tropical circulation patterns or cross-equatorial moisture and energy transport well. Therefore we revisit the response of the North African monsoon to separate precession and obliquity forcings using the fully coupled state-of-the-art general circulation model (GCM) EC-Earth. Our aim is to investigate whether the main conclusions of Tuenter et al. (2003) still hold, by examining in detail which physical mechanisms and feedbacks operate for both orbital parameters, including surface as well as circulation features. EC-Earth is based on a weather forecast model and runs at a resolution of ~1.125° (Hazeleger et al. 2010, 2011). The higher resolution and more sophisticated parametrizations of EC-Earth compared to EC-Bilt result in a much more reliable representation of the monsoonal precipitation and related circulation patterns. Moreover, EC-Earth has been shown to respond well to Mid-Holocene orbital forcing compared to PMIP2 model studies by Bosmans et al. (2012), in which a detailed account of Mid-Holocene monsoons on both hemispheres is given.

This paper is set up as follows: in Sect. 2 the EC-Earth model and the experiments are described. The precession-induced changes in the North African monsoon are

described in Sect. 3.1, followed by the obliquity-induced changes in Sect. 3.2. A discussion and conclusion is presented in Sect. 4.

2 Model and experiment set-up

2.1 The model: EC-Earth

EC-Earth is a fully coupled ocean–atmosphere general circulation model (GCM, Hazeleger et al. 2010, 2011). The atmospheric part of EC-Earth 2.2 is based on the integrated forecasting system (IFS), cycle 31R1, of the European Centre for Medium-range Weather Forecast (ECMWF). Its spectral horizontal resolution is T159 (roughly 1.125° × 1.125°) with 62 vertical levels. IFS cycle 31R1 is improved by adding the Bechtold et al. (2008) convection scheme and the Balsamo et al. (2009) land surface scheme H-TESSEL, including surface runoff. The ocean part consists of Nucleus for European Modelling of the Ocean (NEMO), version 2, running at a horizontal resolution of nominally 1° with 42 vertical levels (Madec 2008; Sterl et al. 2011). NEMO includes the sea-ice model LIM2. The ocean, sea-ice, land and atmosphere are coupled through the OASIS3 coupler (Valcke and Morel 2006).

EC-Earth performs well for the present-day compared to CMIP3 models and data in terms of climatology as well as interannual, spatial and temporal variability (Hazeleger et al. 2010, 2011). More importantly, we have previously shown that monsoonal precipitation is represented well in EC-Earth in both a pre-industrial and a Mid-Holocene paleo-experiment compared to PMIP2 model studies (Bosmans et al. 2012).

2.2 Experimental set-up: insolation forcing and boundary conditions

In order to examine the separate precession and obliquity (tilt) signals we have performed four idealized experiments with different orbital parameters:

Pmin: Minimum precession, minimum obliquity
Pmax: Maximum precession, minimum obliquity
Tmax: Maximum obliquity with a circular orbit
Tmin: Minimum obliquity with a circular orbit.

The values of the orbital parameters are given in Table 1. These are the same as the P−T−, P+T−, P0T+, P0T− experiments in Tuenter et al. (2003), and are based on the extreme values of the orbital parameters occurring in the last 1 Ma (Berger 1978). For precession, extremes of the precession parameter $e\ \sin(\pi + \tilde{\omega})$ are chosen rather than extremes of $\sin(\pi + \tilde{\omega})$, as eccentricity e modulates precession. $\tilde{\omega}$ is the longitude of perihelion, defined as the angle from the vernal equinox to perihelion, measured counterclockwise. We did not perform the precession experiments with maximum obliquity (P−T+ and P+T+ in Tuenter et al. 2003) due to lack of computing time. Furthermore, Tuenter et al. (2003) have shown that the precession signal (in the African monsoon) is not dependent on obliquity. The obliquity signal does depend on the prevailing precession (Tuenter et al. 2003), i.e. comparing P−T+ to P−T− gives different results than comparing P+T+ to P+T−. In this study we fully exclude precession in the obliquity experiments by setting eccentricity to zero (i.e. prescribing a circular orbit).

Table 1 Overview of the orbital configuration in each experiment. Obl is the obliquity (tilt), $\tilde{\omega}$ is the longitude of perihelion, defined as the angle from the vernal equinox to perihelion, measured counterclockwise

Experiment	Obl (°)	$\tilde{\omega}$ (°)	e	$e\ \sin(\pi + \tilde{\omega})$
Pmin	22.08	95.96	0.056	−0.055
Pmax	22.08	273.5	0.058	0.058
Tmax	24.45	–	0	0
Tmin	22.08	–	0	0

e is eccentricity. $e\ \sin(\pi + \tilde{\omega})$ is the precession parameter. Note that for Tmax and Tmin there is no precession because of the circular orbit ($e = 0$)

During a precession minimum (Pmin) the summer solstice occurs at perihelion and the precession parameter $e\ \sin(\pi + \tilde{\omega})$ is negative. Seasonality is enhanced in the northern hemisphere (NH) and reduced in the southern hemisphere (SH). The opposite occurs during a precession maximum (Pmax), when the summer solstice occurs at aphelion and the precession parameter $e\ \sin(\pi + \tilde{\omega})$ is at its maximum value. Figure 1a shows the insolation differences between Pmin and Pmax, calculated using the equations of Berger (1978). During an obliquity maximum (Tmax, maximum tilt), both NH and SH summers receive more insolation, especially at the poles, while during an obliquity minimum (Tmin) summer insolation is reduced. The obliquity-induced insolation changes are shown in Fig. 1b. The orbital parameters, shown in Table 1, are kept fixed during each experiment. All other boundary conditions (e.g. the solar constant, greenhouse gas concentrations, orography, ice sheets, vegetation) were kept constant at pre-industrial levels. We keep vernal equinox fixed at the 21st of March and use the present-day calendar. This introduces some errors in the precession experiments, because the lengths of the seasons and the dates of the equinoxes and solstices change along the precession cycle (Joussaume and Braconnot 1997). A celestial calendar, using angular months based on astronomical

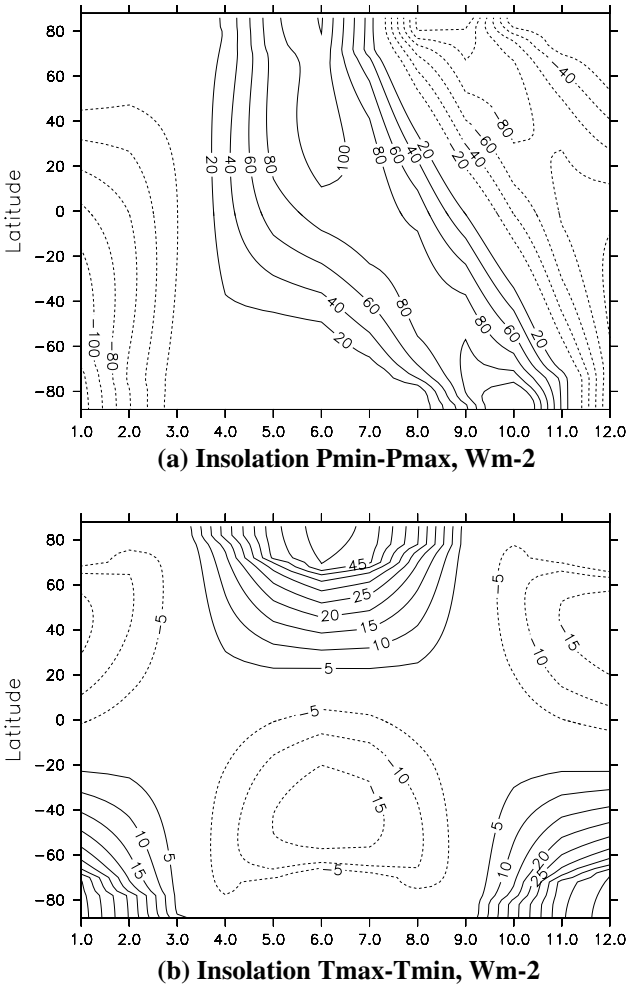

Fig. 1 Insolation differences at the top of the atmosphere (TOA): precession minimum minus maximum (**a**, *contour* interval 20 Wm^{-2}) and obliquity (tilt) maximum minus minimum (**b**, *contour* interval 5 Wm^{-2}). See Table 1 for the values of the orbital parameters. Insolation is calculated for every second latitude and every month (mid-month)

positions, would be more appropriate. However, because Tuenter et al. (2003), and others (e.g. Braconnot et al. 2008; Chen et al. 2011), also use the present-day calendar, we maintain this calendar to facilitate comparison.

EC-Earth is computationally expensive. Each experiment was run for 100 years, initiated from a pre-industrial experiment (Hazeleger et al. 2011). The first 50 years are considered spin-up. The experiments are long enough for atmospheric and surface variables that are of interest to monsoon dynamics to equilibrate to the forcing (Fig. 2). Annual mean temperatures drop in the first ~10 years, then level off. Temperatures in the Tmax experiment show a relatively strong cooling trend (Fig. 2a, b), but these trends do not cause a trend in the tropical monsoonal precipitation (Fig. 2d). Table 2 shows the trends for both the zonal mean (as shown in Fig. 2) and for Africa, where trends are slightly larger (likely related to focussing on a smaller area). The globally averaged tendency term of surface air temperature, *dT*/*dt*, is near-zero and shows no trend in all experiments (not shown). Precipitation over the tropical land areas, an indication of monsoon precipitation, shows virtually no trend (Fig. 2d). Furthermore, taking the last 30 years instead of the last 50 years does not influence the results (not shown).

3 Results

In this section we focus on the North African summer monsoon, investigating in detail the changes in the monsoon precipitation, temperature, surface wind and pressure, moisture transport and large-scale circulation induced by precession (Sects. 3.1.1–3.1.5) and obliquity (Sects. 3.2.1–3.2.5). We compare Pmin–Pmax and Tmax–Tmin, i.e. maximum to minimum boreal summer insolation, using June–July–August averages. The figures also give results for each experiment separately. The response of the Asian summer monsoons and the Mediterranean region will be discussed in separate papers.

3.1 The North African Monsoon: precession

3.1.1 Precession: precipitation

During boreal summer, insolation is higher in both hemispheres in the Pmin experiment than in Pmax. Insolation differences reach over 100 Wm^{-2} (Fig. 1a). There are large differences in precipitation over North Africa during the summer monsoon between Pmin and Pmax (Fig. 3). In the Pmin experiment, summer precipitation maxima occur over the continent at 5–5°N, with rates of 10 mm/day and higher. Precipitation extends far north into the Sahara; the 1 mm/day contour extends up to 20–25°N in the north-eastern Sahara and up to the Atlas mountains in the west (Fig. 3). In the Pmax experiment, summer precipitation occurs mostly over the Atlantic, while over land the precipitation rate is only 2–6 mm/day over the south-western coast. Precipitation does not extend farther north than 15°N.

The difference between Pmin and Pmax is also evident from the yearly cycle of precipitation over tropical North Africa, shown in Fig. 4a. Summer monsoonal precipitation is much larger in Pmin, reaching over 8 mm/day (averaged over 10°W:40°E, 5°N:20°N). In Pmax, the summer precipitation over the continent is small, and in contrast to Pmin, precipitation maxima occur in spring and autumn, not summer (Fig. 4a). This suggests that

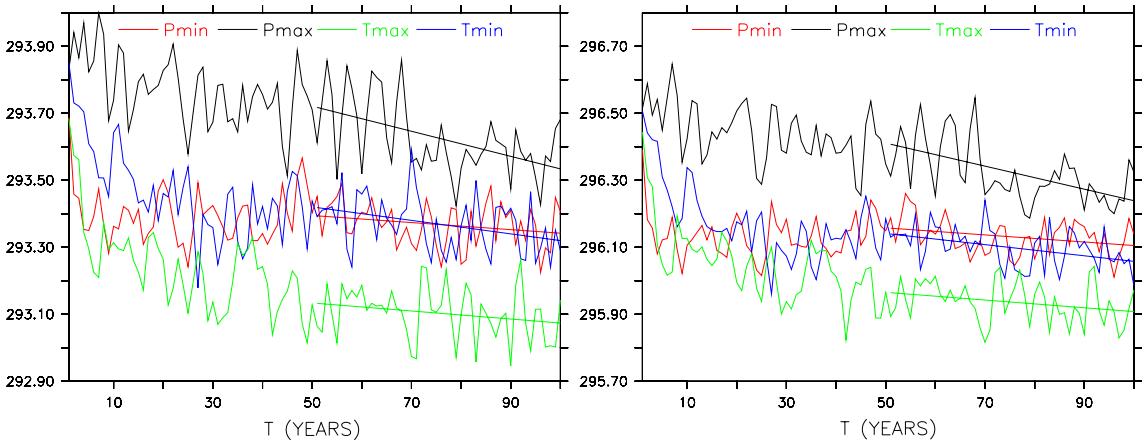

(a) Surface air temperature, K

(b) Sea surface temperature, K

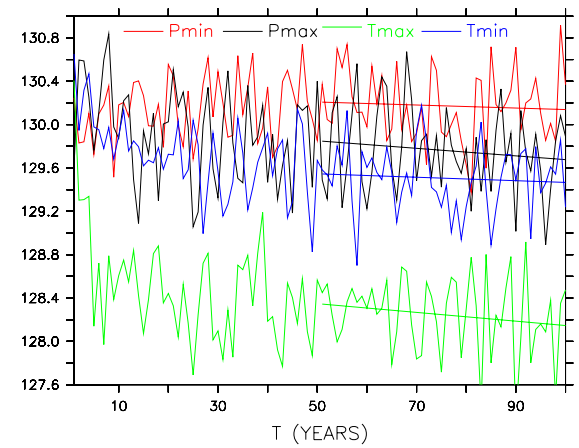

(c) Surface heat flux, Wm-2

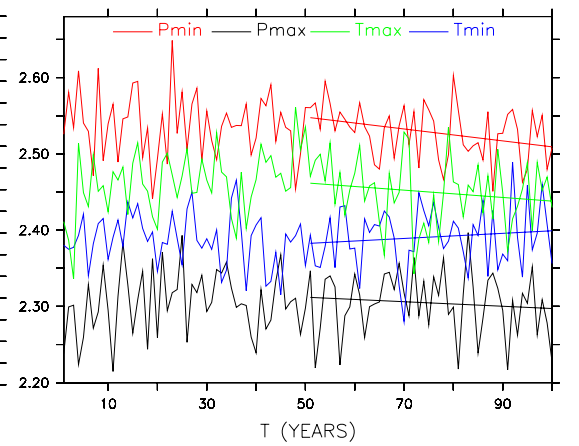

(d) Precipitation, land only, mm/day

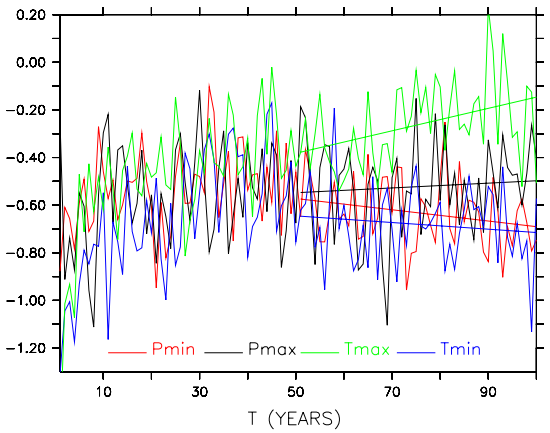

(e) TOA net radiative flux, Wm-2

Fig. 2 Annual mean surface air temperature (**a**), sea surface temperature (**b**), sum of surface sensible and latent heat fluxes (**c**) and total (convective + large scale) precipitation (**d**) in all four experiments zonally averaged over 40°S:40°N. Top-of-atmosphere annual global mean net radiative flux (net shortwave plus net longwave radiation) is given in (**e**). *Trend lines* over the last 50 years are added in each figure (calculated using linear regression). Values of the trends are given in Table 2

precipitation responds strongly to the local insolation forcing over the tropics, which also has a single strong peak in summer in Pmin and two peaks in spring and autumn in Pmax (Fig. 4c). North of the Tropic of Cancer both Pmin and Pmax show a single summer insolation peak.

Table 2 Trends over tropics (40°N:40°S, zonal mean, as shown in Fig. 2) and Africa (40°N:40°S, 10°W:40°E), based on annual means of the last 50 years of the experiments

	Pmin	Pmax	Omax	Omin
Surface air temperature tropics	−1.06E−3	−3.75E−3	−1.20E−3	−2.01E−3
Surface air temperature Africa	−2.10E−3	−4.35E−3	−6.73E−4	−3.07E−3
Sea surface temperature tropics	−1.06E−3	−3.44E−3	−1.15E−3	−1.67E−3
Sea surface temperature Africa	−5.23E−3	−4.94E−3	−1.78E−3	−1.68E−3
Surface heat flux tropics	−1.40E−3	−3.48E−3	−4.04E−3	−1.59E−3
Surface heat flux Africa	−5.45E−3	−1.17E−2	−1.27E−2	9.65E−3
Precipitation tropics	−7.81E−4	−2.98E−4	−4.79E−4	3.35E−4
Precipitation Africa	−1.16E−3	−4.40E−4	−1.40E−3	8.42E−4
TOA net radiative flux global	−2.37E−3	1.01E−3	4.72E−3	−1.40E−3
TOA net radiative flux Africa	−1.95E−3	4.81E−3	4.01E−3	−1.13E−3

For precipitation only land grid points are used. Note that for sea surface temperature (SST) the trend is calculated over 40°N:40°S, 40°W:40°E. Trends are given in °C/year for surface air and sea surface temperature, W/m^2/year for the surface heat flux and TOA net radiative flux, and mm/day/year for precipitation

3.1.2 Precession: temperature and energy balance

To further investigate the differences between Pmin and Pmax, we look into changes in temperature, the surface energy balance, pressure, and winds at the surface. Figure 5 shows that JJA surface air temperatures are higher in the Pmin experiment, especially over land, with the exception of the continental monsoon region. There, temperatures are up to 5° lower, which can be explained by feedbacks from monsoon intensification. Increased cloud cover reduces the surface downward shortwave radiation by 59.3 Wm^{-2} (averaged over 10°W:40°E, 5°N:20°N, JJA, land only), despite the ∼90 Wm^{-2} increase in downward shortwave radiation at the top of the atmosphere. Also, increased evaporation leads to an increased surface latent heat flux of 52.9 Wm^{-2} (a difference of more than 150 %). These changes are only partly compensated by increased surface downward thermal radiation due to increased cloud cover (49.8 Wm^{-2}) and decreased surface upward shortwave radiation (14.0 Wm^{-2}). Due to the cooler surface, there is a smaller surface sensible heat flux (37.9 Wm^{-2}) and less surface upward thermal radiation (11.6 Wm^{-2}), see Fig. 6. These changes in the surface energy balance completely counteract the direct warming effect of increased insolation.

In the Pmin experiment, sea surface temperatures are generally higher in summer due to increased insolation (not shown), but the changes are smaller than over land due to the ocean's larger heat capacity. Near the south-west coast of North Africa SSTs are lower in Pmin. Increased winds over this coastal region (Fig. 8) create stronger upwelling, cooling the surface and reducing evaporation.

3.1.3 Precession: surface wind and pressure

The increased monsoonal winds into North Africa respond to changes in surface pressure. Figure 7 illustrates that the low pressure areas over the Sahara are stronger and located further north in the Pmin experiment, as a result of the strong surface warming in the (northern) Sahara (Fig. 5). Surface pressure in JJA is reduced by up to 8 hPa over the north-eastern Sahara, associated with intensified heat lows, and up to 7 hPa over the north-western coast, where the Azores High is shifted northwestward. Over continental tropical eastern North Africa surface pressure is increased, related to the northward shift of the Saharan low pressure areas and the decreased surface temperature. Therefore the insolation changes do not induce a simple intensification of the land–sea pressure difference. In response to the stronger low pressure areas, located farther north over the Sahara, the monsoon winds are stronger and penetrate further north (Fig. 8). Northerly winds into the north-eastern Sahara are stronger as well, so the convergence of northerly and southerly winds is stronger. Also, a stronger South-Atlantic subtropical high further increases the pressure gradient between the (southern) Atlantic and the northern Sahara, causing more southerly winds to cross the equator into the monsoon area. Near the west coast, the northerly trade winds at 10–20°N are turned more landward in Pmin.

3.1.4 Precession: moisture sources

Over the continent, changes in local recycling play only a small role in the increased precipitation; evaporation is increased by only 2–3 mm/day (Fig. 9). Although this evaporation increase plays an important role in lowering the surface temperature (Sect. 3.1.2), the changes are not large enough to explain the precipitation changes (up to 10–12 mm/day, Fig. 3). Calculating $(\Delta P – \Delta E)/\Delta P$, where Δ is the Pmin–Pmax difference for 10°W:40°E, 5°N:20°N, land only, shows that during JJA, to first order, 72 % of the precipitation increase originates from outside this area. Increased evaporation over the nearby Atlantic could explain enhanced moisture advection into North Africa. However, evaporation is reduced at 10–20°N over the Atlantic (Fig. 9), where the northerly trade winds turn more landward and lose some of their speed. Near the

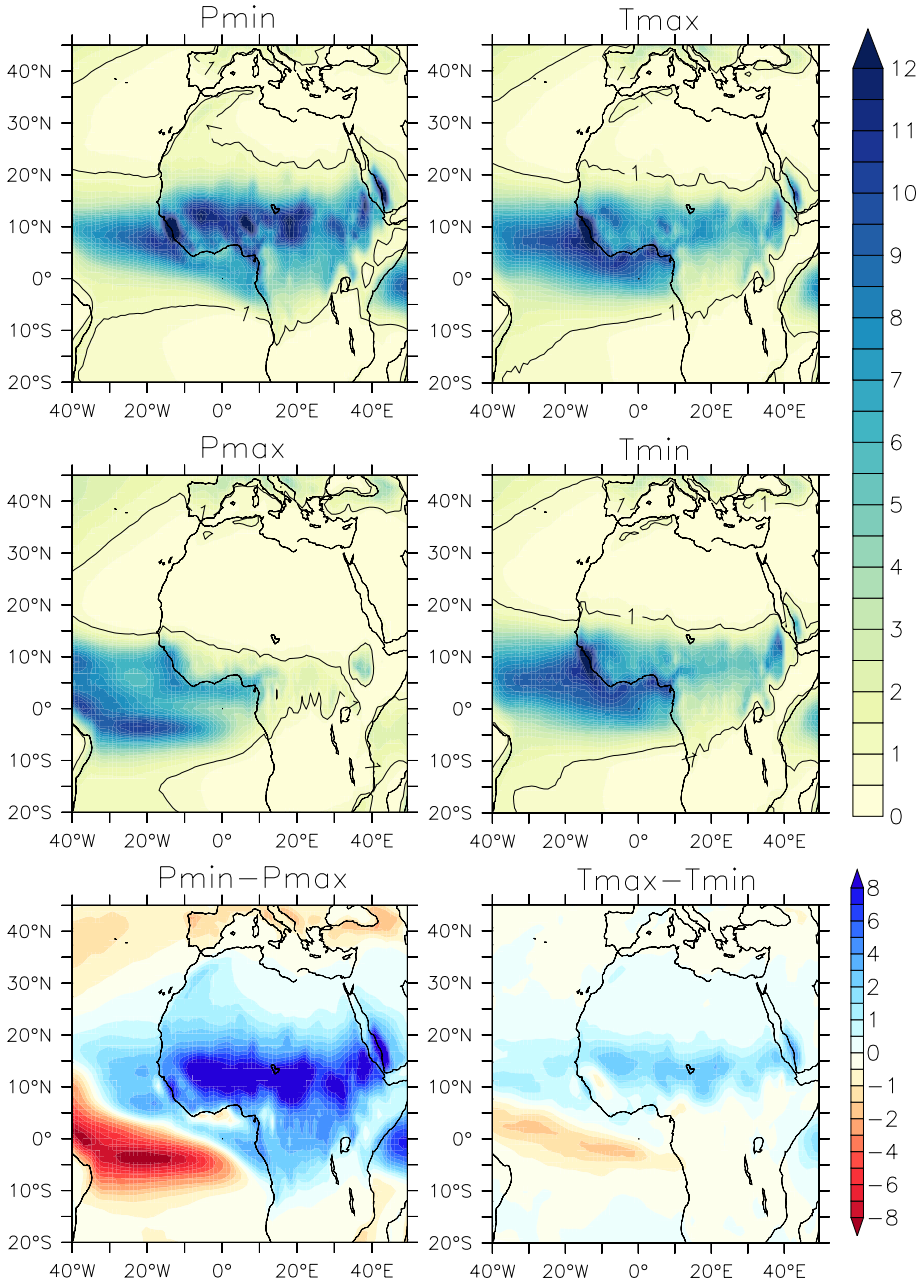

Fig. 3 June–July–August average precipitation in mm/day in the Pmin experiment (*top left*), Pmax (*mid left*), Tmax (*top right*), Tmin (*mid right*) and the Pmin–Pmax differences (*lower left*) and Tmax–Tmin differences (*lower right*)

south-western coast evaporation is reduced as well, due to increased upwelling and lower SSTs. Over the western tropical Atlantic there is an increase in evaporation (up to 1.5 mm/day) which, together with the decrease in precipitation (up to 8 mm/day) over the south-western tropical Atlantic (Figs. 3, 9), could leave more moisture available for transport into the continental monsoon area. Figure 10 shows the changes in moisture transport **Q**, the mass-weighted vertical integral of specific humidity q multiplied by horizontal wind **v**. The moisture transport into North Africa from the Atlantic over the southwestern coast is indeed increased. Changes in total moisture transport **Q** are composed of three terms:

$$\Delta\mathbf{Q} = \frac{1}{g}\int_{p_s}^{p_0} \Delta(q\mathbf{v})\,\mathrm{d}p = \frac{1}{g}\left(\int_{p_s}^{p_0} \mathbf{v}\Delta q\,\mathrm{d}p + \int_{p_s}^{p_0} q\Delta\mathbf{v}\,\mathrm{d}p + \int_{p_s}^{p_0} \Delta q\Delta\mathbf{v}\,\mathrm{d}p\right) \quad (1)$$

where $\mathbf{v}\Delta q$ is the thermodynamic part (due to changes in specific humidity with fixed winds), $q\Delta\mathbf{v}$ is the dynamic part (due to changes in winds with fixed humidity) and $\Delta q\Delta\mathbf{v}$ is due to changes in both winds and humidity. p_s is surface pressure, p_0 is the top of the atmosphere. These three terms are shown in Fig. 11. Most of the increased moisture transport is related to increased winds (Fig. 8); the dynamic term $q\Delta\mathbf{v}$ dominates the moisture transport into

North Africa and across the equator (Fig. 11). Therefore the reduced precipitation over the tropical Atlantic is likely a consequence of the enhanced landward moisture transport. Furthermore, changes in net precipitation, P–E, shown in Fig. 10, are very similar to the changes in precipitation (Fig. 3), again illustrating that evaporation changes do not play a large role.

Over the Sahara, at ∼20–30°N the thermodynamic term $\mathbf{v}\Delta q$ also plays an important role, because Δq is largest over this area (not shown). Increased precipitation over northwestern North Africa (Fig. 3) is therefore due to both an increased wind from the east ($q\Delta\mathbf{v}$) and advection of increased specific humidity ($\mathbf{v}\Delta q$, Fig. 10). Moisture transport from the Atlantic trade winds, which are are less landward in Pmin, is weakened. Local recycling also plays an important role over northwestern North Africa; (ΔP $-\Delta$E)/ΔP over 15°W:0°E, 25°N:35°N, land only, is 25 %.

3.1.5 *Precession: large-scale circulation*

Not only do horizontal winds change, but there are also large changes in vertical velocity. Most of the monsoon precipitation is convective, so it is no surprise that ascending motion over land is increased while over the ocean ascending motion is reduced (Fig. 12). In the Pmin experiment, maximum upward vertical velocity occurs over the continent at 10–15°N at 400–500 hPa height, extending north up to 20°N, while in Pmax there is little vertical velocity at this height over land and maxima of vertical velocity lie mostly over the tropical Atlantic (Fig. 12). Therefore, like precipitation, convection (ascending motion) shifts from ocean to land in Pmin. Furthermore, convection over continental tropical Africa follows the local insolation forcing and shows a double peak in spring and autumn in Pmax, and a single peak in summer in Pmin (Figs. 4a for

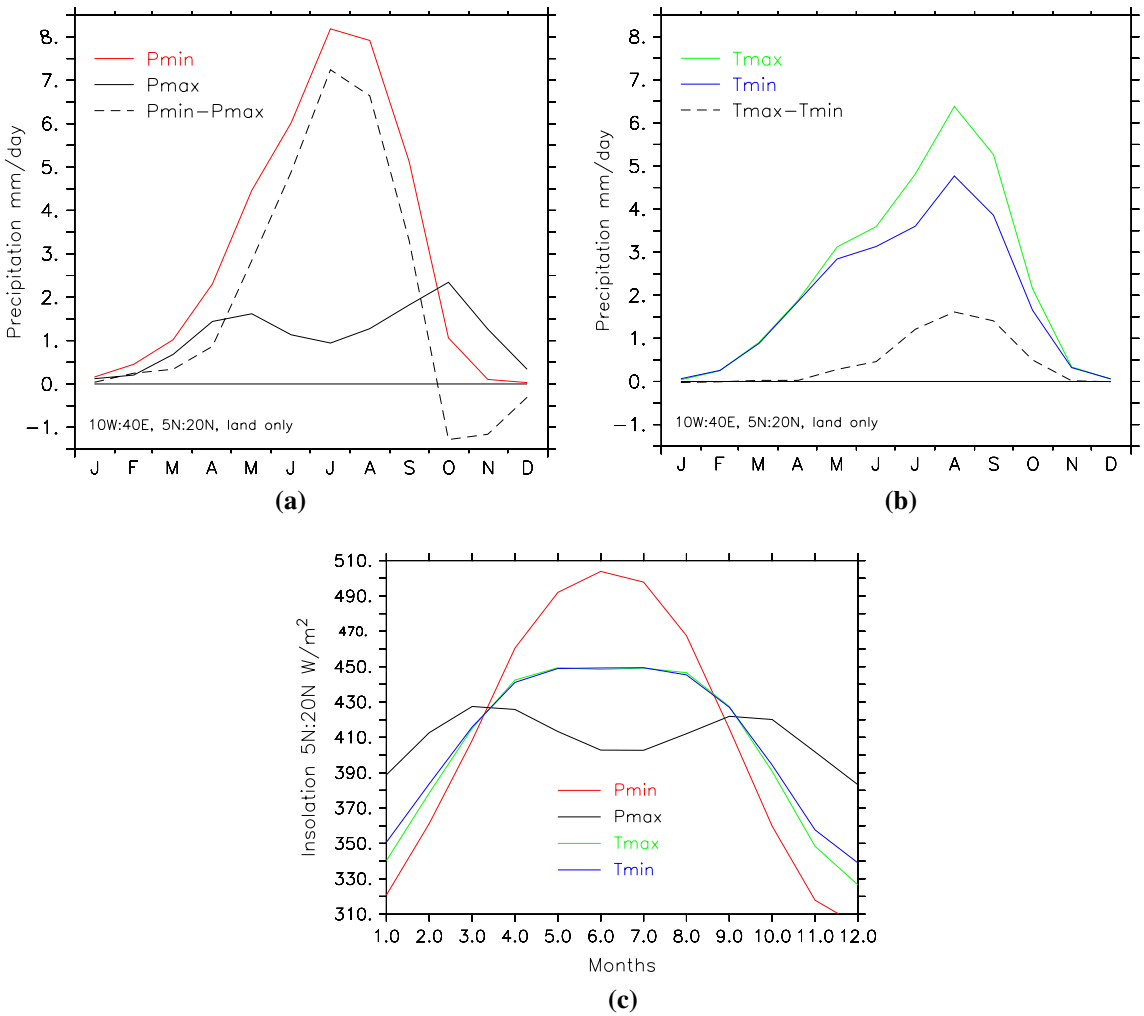

Fig. 4 Precipitation over North Africa, land only, in mm/day for precession (**a**) and obliquity (**b**), averaged 10°W:40°E, 5°N−20°N. Differences are given by the *dashed lines*. Insolation over the tropics (5–20°N averaged, W/m^2) is given in (**c**) for each experiment

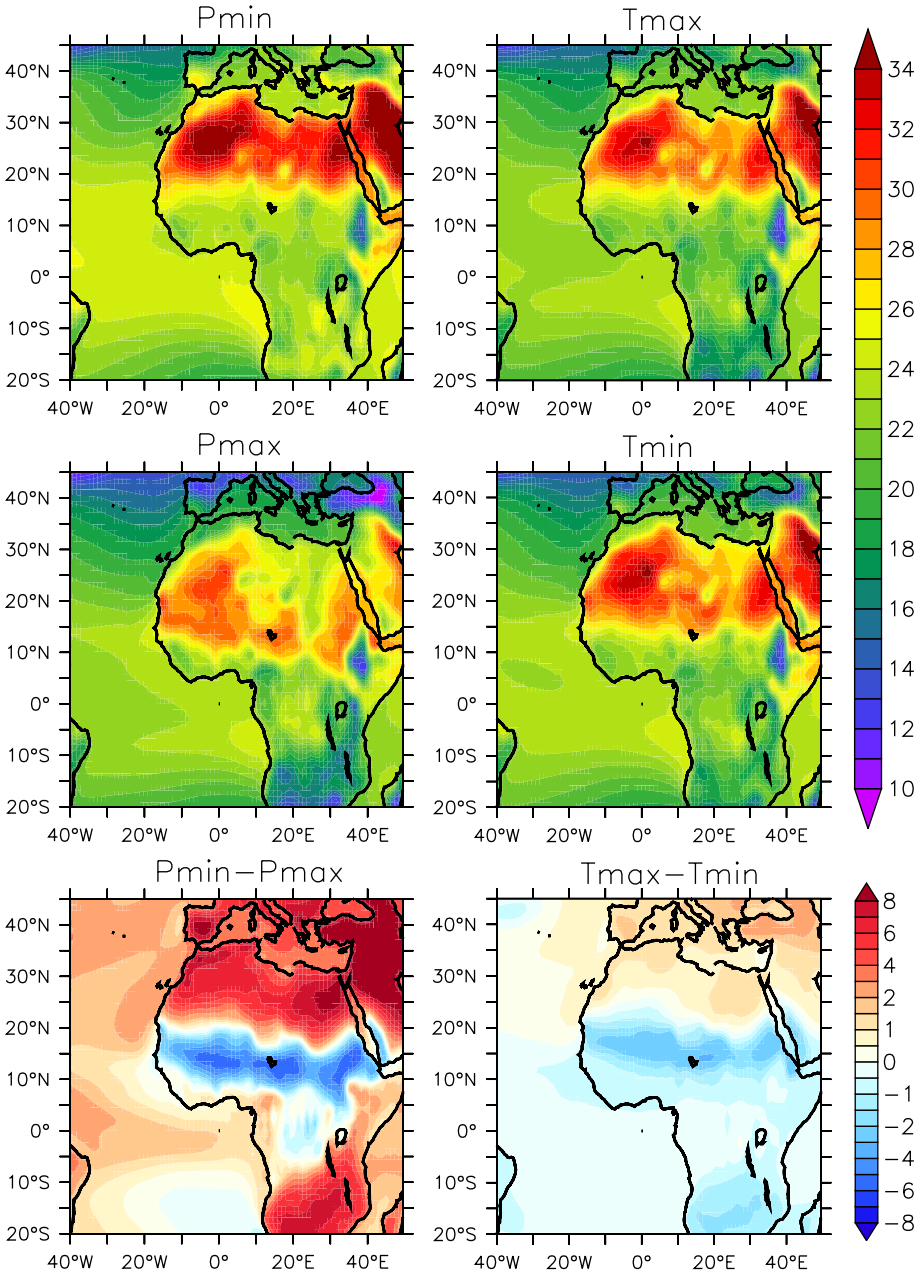

Fig. 5 June–July–August average surface air temperature in °C in the Pmin experiment (*top left*), Pmax (*mid left*), Tmax (*top right*), Tmin (*mid right*) and the Pmin–Pmax differences (*lower left*) and Tmax–Tmin differences (*lower right*)

precipitation and 4c for insolation). Over the north-eastern Sahara, subsidence is weaker in Pmin in summer.

The northward extension of convection is also evident in Fig. 13, which shows 30°W:40°E zonally averaged vertical motion. In the Pmin experiment, deep convection occurs at 10–15°N, consistent with high precipitation at this latitude (Fig. 3). Shallow convection occurs at 20–25°N, overlying the low pressure areas where northward monsoon winds meet southward winds from the Mediterranean (Figs. 7, 8). In the Pmax experiment, shallow convection occurs at 10–15°N (Fig. 13), mostly over eastern Africa (not shown). Deep convection occurs over the Atlantic, where precipitation is strongest in Pmax (Figs. 3, 12). In agreement with the northward extension of convection in Pmin the African Easterly Jet (Nicholson 2009) is located further north, at 15–20°N and 500 hPa (Fig. 13). In Pmax, the AEJ is located at 5–10°N and 600–700 hPa, but it is stronger (not shown), further decreasing the moisture content over continental North Africa.

3.2 The North African Monsoon: obliquity

3.2.1 Obliquity: precipitation

The obliquity-induced insolation changes over the tropics during boreal summer are small, (<5 Wm^{-2} or <1 % for

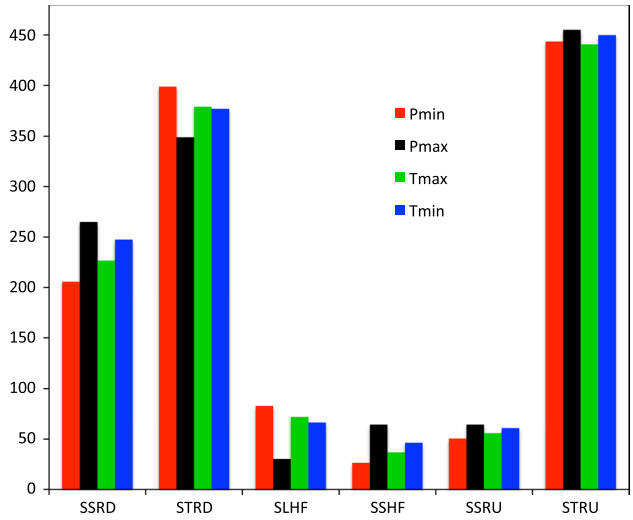

Fig. 6 Overview of surface energy balance terms per experiment and differences, averaged over 10°W:40°E, 5°N:20°N, JJA, land only, in W/m^2. SSRD is surface shortwave radiation downward, STRD is surface thermal (longwave) radiation downward, SLHF is surface latent heat flux, SSHF is surface sensible heat flux, SSRU is surface shortwave radiation upward, STRU is surface thermal (longwave) radiation upward. Note that absolute values are shown; SSRD and STRD are fluxes from the atmosphere towards the surface, while SLHF, SSHF, SSRU and STRU are fluxes from the surface towards the atmosphere

JJA 0°N:30°N, Figs. 1b, 4c). Nonetheless, there is a clear obliquity-induced precipitation change (25 %, averaged over 0°N:30°N, 20°W:50°E, land only, JJA). This precipitation change (Fig. 3) must therefore either originate at higher latitudes, as suggested by Tuenter et al. (2003), be related to non-linear responses, or be induced by changes in the inter-hemispheric insolation gradient, which is stronger in the Tmax experiment when NH summer insolation is increased and SH winter insolation is decreased. The JJA averaged insolation gradient between 23°N and 23°S is 17.5 Wm^{-2} stronger in Tmax.

The climatologies of Tmax and Tmin are overall much more alike than those of Pmin and Pmax, because of the small insolation differences over the tropics. For precipitation, the annual cycle is slightly stronger in the Tmax experiment (Fig. 4b). Precipitation extends further north in Tmax, reaching just over 20°N (based on the 1 mm/day contour for JJA, Fig. 3). Precipitation is also increased over the Atlas mountains. In Tmin, precipitation reaches 15–20°N. Over land, the differences are up to 2–3 mm/day at 10–15°N (Fig. 3).

3.2.2 *Obliquity: temperature and energy balance*

Changes in temperature show a meridional pattern, see Fig. 5. Temperatures on the southern hemisphere are reduced due to reduced insolation, while on the northern hemisphere temperatures are increased due to increased insolation. Over North Africa, increased temperatures extend up to 20–25°N, as the surface of monsoonal North Africa is cooled through feedbacks within the monsoon system, similar to the response to precession, see Sect. 3.1. There is a reduction in surface downward shortwave radiation of 20.7 Wm^{-2} (an order of magnitude larger than the local insolation increase) due to increased cloudiness and a stronger surface latent heat flux of 5.5 Wm^{-2} due to increased evaporation (Fig. 6), resulting in surface temperatures of up to 3 °C lower. Sea surface temperatures (not shown) show a response very similar to surface air temperature, with further lowering of SSTs along the coast of North Africa due to increased upwelling related to increased surface winds.

3.2.3 *Obliquity: surface wind and pressure*

Pressure changes closely follow the temperature changes (Fig. 7). Pressure is up to 2 hPa lower over the north-eastern Sahara as well as over the western coast, where the Azores High is weakened. The monsoon winds are stronger and drawn slightly further north in response to the reduced pressure over the northern Sahara, (Figs. 7, 8). A strengthened South Atlantic subtropical high strengthens the cross-equatorial pressure gradient and forces more southerly cross-equatorial winds into the monsoon region, in agreement with a stronger cross-equatorial insolation gradient.

3.2.4 *Obliquity: moisture sources*

Similar to the monsoonal response to precession, precipitation is shifted from ocean to land (Fig. 3). Indeed, moisture transport $\mathbf{Q}$ is increased over the south-west coast into North Africa (Fig. 10). Most of the increased moisture transport is due to wind changes ($q\Delta\mathbf{v}$, the dynamic term in Eq. 1, see Fig. 11). A small part of this increase comes from the southern tropical Atlantic due to the stronger cross-equatorial southerly winds. Terms $\mathbf{v}\Delta q$ and $\Delta q\Delta\mathbf{v}$ are small south of ~10°N and act to reduce northward moisture transport, because Δq is negative as a result of decreased JJA insolation south of ~10°N. Compared to the increased moisture transport from the tropical Atlantic, changes in moisture transport from the north are small (Fig. 10) due to both small changes in winds and small changes in humidity north of the monsoon region. Over northwestern North Africa, moisture transport is more north-westward in the Tmax experiment and moisture transport in the trades is weaker (Fig. 10). Increased precipitation over north-westernmost North Africa (Fig. 3) is therefore related to increased moisture transport from the Sahara and northern monsoon region, as well as increased evaporation; $(\Delta P - \Delta E)/\Delta P$ is 14 % over 15°W:0°E, 25°N:35°N (land only).

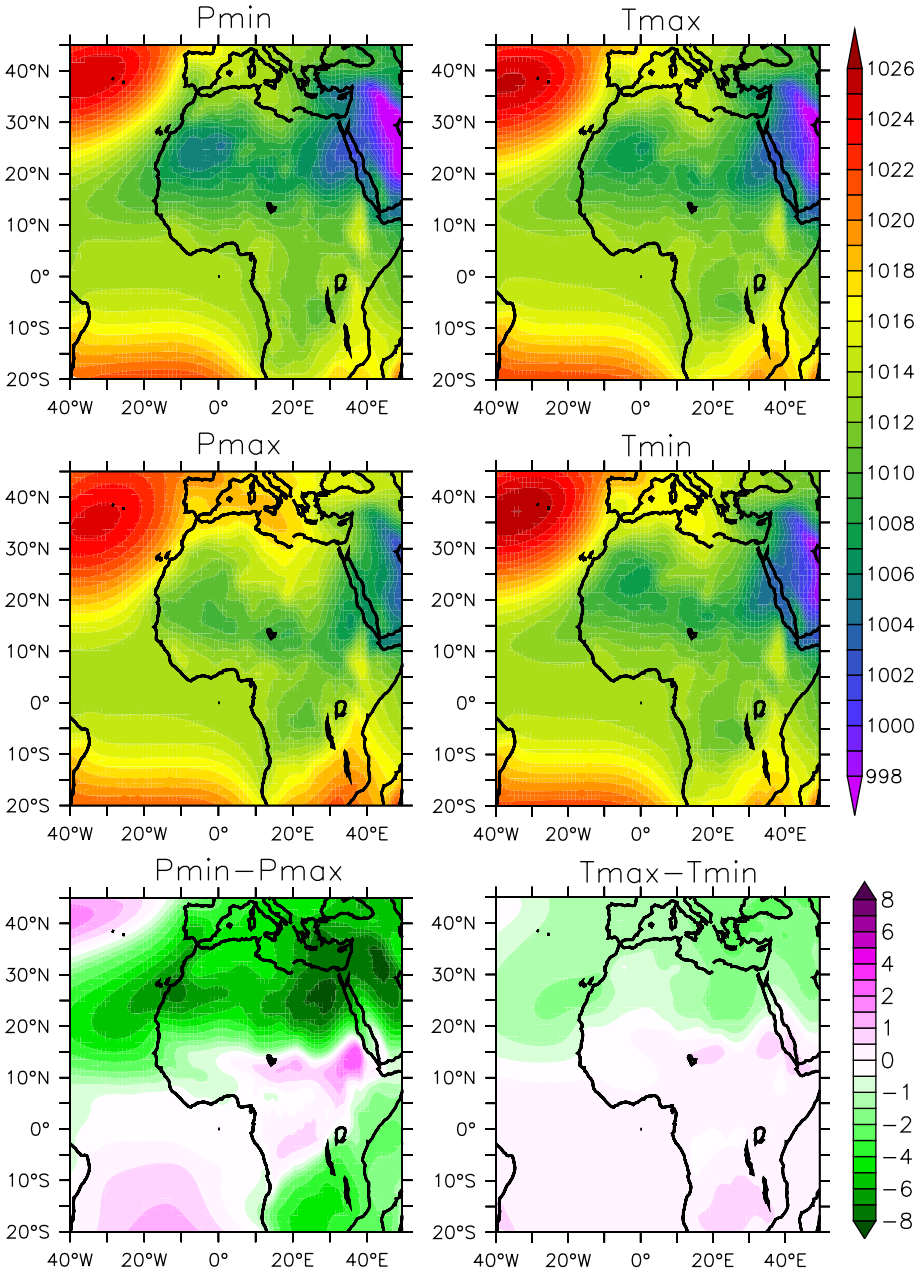

Fig. 7 June–July–August average sea level pressure in hPa in the Pmin experiment (*top left*), Pmax (*mid left*), Tmax (*top right*), Tmin (*mid right*) and the Pmin–Pmax differences (*lower left*) and Tmax–Tmin differences (*lower right*)

Over the monsoon region, increased moisture advection is the main reason for increased precipitation. $(\Delta P - \Delta E)/\Delta P$ is 81 % (for 10°W:40°E, 5°N:20°N, land only). The pattern of changes in net precipitation, P–E, is very similar to the pattern of changes in precipitation (Figs. 3, 10), further indicating that evaporation changes are of minor importance within the monsoon region.

3.2.5 Obliquity: large-scale circulation

Changes in large-scale circulation are evident from changes in vertical motion. Like precipitation, convection in Tmax is increased over land, extending slightly further north, and decreased over the ocean (Fig. 12). Convection is reduced over the Atlas mountains; local recycling explains most of the precipitation increase. Decreased subsidence occurs over the north-eastern Sahara and eastern Mediterranean. Figure 13 also shows that ascending motion extends further north in Tmax. Strong convection occurs just north of 10°N in Tmax and just south of 10°N in Tmin, in line with maximum precipitation at these latitudes (Fig. 3). Shallow convection overlies the surface lows at ~20°N, which are located slightly further north in Tmax. Furthermore, the African Easterly Jet is located further north in Tmax, consistent with the northward extension of ascending motion.

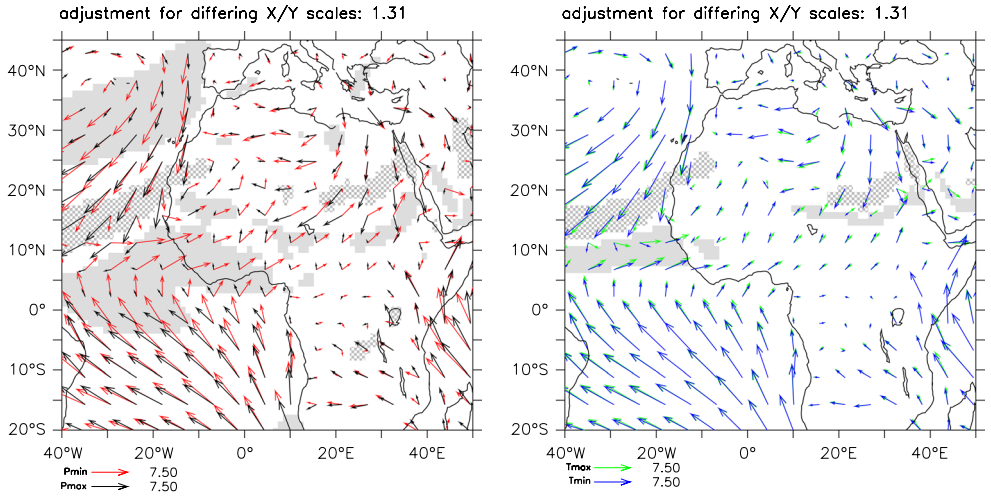

Fig. 8 June–July–August average surface winds in m/s in the Pmin experiment (*left, red*), Pmax (*left, black*), Tmax (*right, green*), Tmin (*right, blue*). Differences in wind speed are given by *grey shading*; *solid* (*chequered*) for *larger* (*smaller*) wind speeds during Pmin and Tmax, shown are differences larger than 2 m/s for precession and 1 m/s for obliquity

4 Discussion and conclusions

This study is the first to investigate the response of the North African monsoon to the separate precession and obliquity signals using a fully coupled, high-resolution GCM (EC-Earth). For both the precession and obliquity experiments, the North African monsoon circulation is strengthened when NH summer insolation is stronger (during minimum precession and maximum obliquity, Pmin and Tmax, see Sect. 2.2). In the Pmin and Tmax experiments monsoonal precipitation is stronger and farther northward due to stronger monsoonal south-westerlies, corresponding to stronger heat lows over the Sahara and a stronger cross-equatorial pressure gradient. The latter is related not only to the stronger Saharan heat lows but also to a stronger South Atlantic subtropical High, especially in the case of precession. More moisture is transported landwards from the tropical Atlantic, mostly by stronger monsoon winds, and precipitation and convection over the ocean are reduced. There is also slightly more moisture advection from the north, but this increase plays a minor role compared with the increased moisture advection from the tropical Atlantic.

The precession-induced insolation changes, much larger than those induced by obliquity, consist of a large increase in insolation during NH summer of up to 100 Wm^{-2}. Consequently monsoon precipitation is increased more in Pmin than in Tmax. Furthermore, the seasonal cycle of insolation over the tropics is rather different in Pmin and Pmax, with a single summer peak in Pmin and two peaks in spring and autumn in Pmax. A similar pattern is seen in the seasonal cycles of precipitation and convection over North Africa, suggesting that precipitation responds strongly to the local insolation forcing.

The obliquity-induced insolation change over the tropics during NH summer is very small (<5 Wm^{-2}). Insolation is increased by 0.27 % in the Tmax experiment, yet precipitation is enhanced by 25 % (averaged over 0°N:30°N, JJA). The cross-equatorial insolation gradient, increased by 17.5 Wm^{-2} in Tmax (23°N:23°S JJA), may therefore play an important role in obliquity-induced climate change. The South Atlantic subtropical high is stronger, pushing more southerly winds into the monsoon region. Specific humidity over the southern Atlantic is lower because of reduced SH austral winter insolation, but stronger north-northeastward monsoon winds result in increased moisture transport from both the southern and northern equatorial Atlantic into the monsoon region. In Pmin, specific humidity over the southern Atlantic is increased during JJA due to higher insolation. Therefore the precession-induced increase in moisture transport into the monsoon region is larger than the obliquity-induced increase, not only because of the stronger response of the monsoonal south-westerlies over the equatorial Atlantic, but also because of increased humidity over the SH.

The increased south-westerly monsoon winds and moisture transport, as well as the redistribution of precipitation from ocean to land is in agreement with previous studies, such as Prell and Kutzbach (1987); Tuenter et al. (2003); Clement et al. (2004); Mantsis et al. (2013); Khon et al. (2010); Erb et al. (2013); Merlis et al. (2013a). Braconnot et al. (2008) furthermore specifies the important role of large-scale dynamics over (local) evaporation. The precession-induced changes in this study are also very similar to the Mid-Holocene monsoon changes (e.g. Braconnot et al. 2007; Bosmans et al. 2012), albeit larger because of high eccentricity. There are small differences in the pattern of

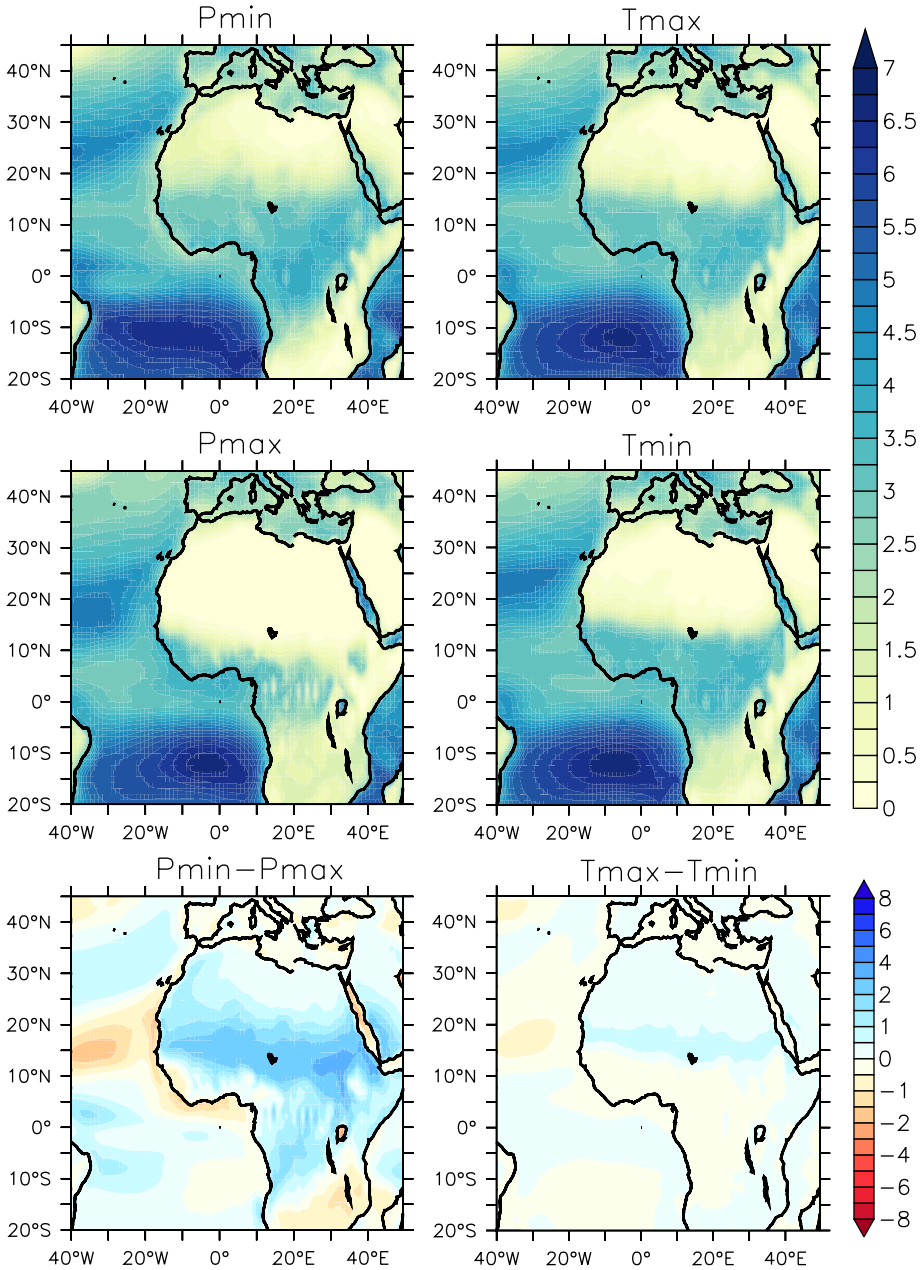

Fig. 9 June–July–August average evaporation in mm/day in the Pmin experiment (*top left*), Pmax (*mid left*), Tmax (*top right*), Tmin (*mid right*) and the Pmin–Pmax differences (*lower left*) and Tmax–Tmin differences (*lower right*)

changes between the precession and Mid-Holocene cases. These may be related to the low eccentricity during the Mid-Holocene and the subsequent low amplitude of precession-induced insolation forcing, i.e. a non-linearity in the response to precession, or to the combined precession and obliquity forcing during the Mid-Holocene. Further sensitivity studies could shed more light on the combined roles of eccentricity, precession and obliquity.

There are differences compared with other studies, however. None of the above-mentioned studies show a summer precipitation increase over north-westernmost Africa, which we find in EC-Earth mostly for precession (and the Mid-Holocene, Bosmans et al. 2012). Given the patterns of wind and moisture transport we suggest that this precipitation increase could be the result of enhanced moisture advection from the monsoon region, opposite to the findings of Laan et al. (2005). However, further investigation is necessary to quantify the role of moisture transport from the Atlantic through low pressure systems, which are not visible in the monthly averages used here, as well as precipitation changes in other seasons. Secondly, Prell and Kutzbach (1987) and Tuenter et al. (2003) suggest that the increased south-westerly monsoon winds into North Africa are remotely forced by reduced pressure over Asia. In EC-Earth we also find a pressure reduction over northern Africa as well as over continental Asia (not shown), but

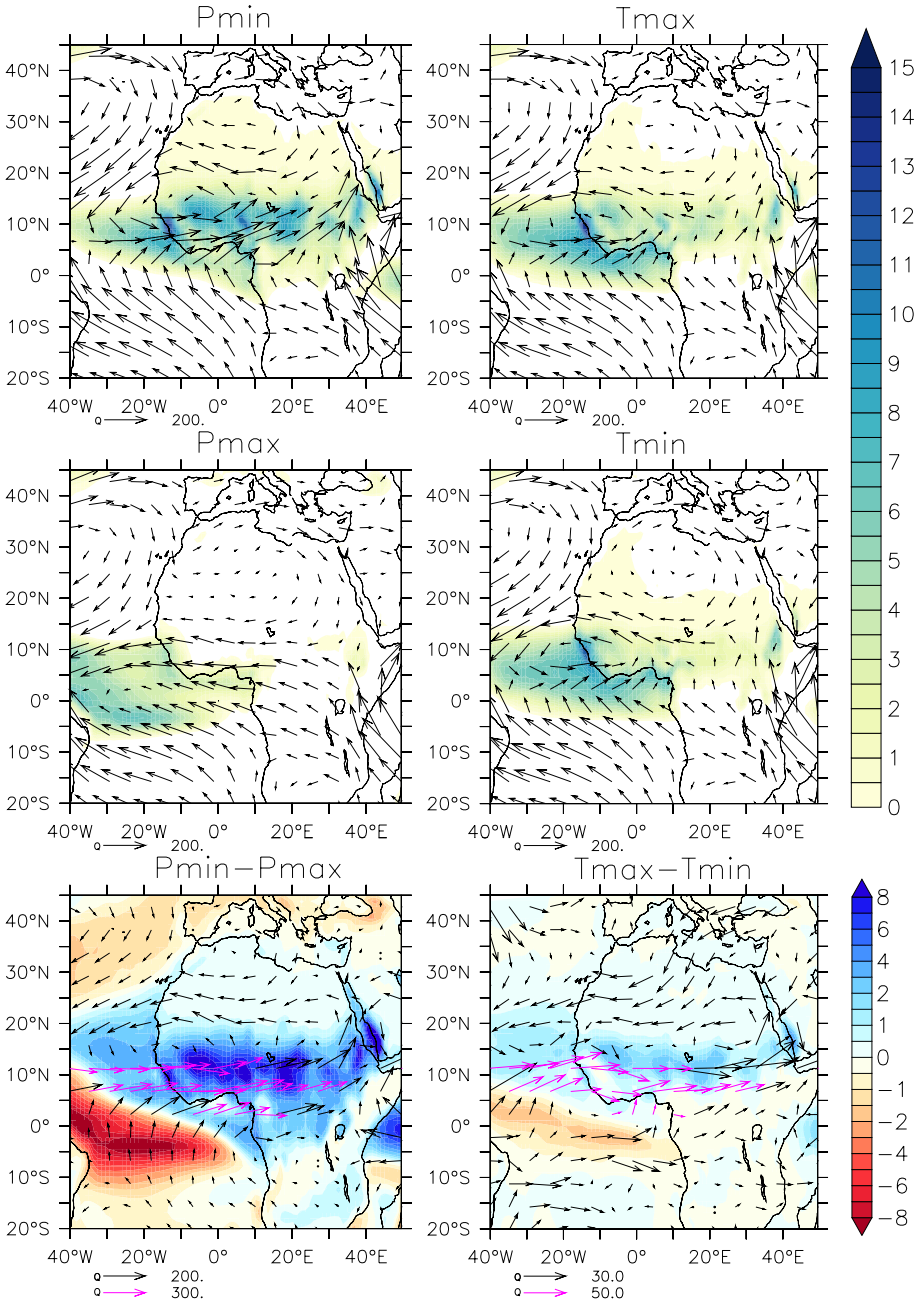

Fig. 10 June–July–August average net precipitation (*colours*) in mm/day in the Pmin experiment (*top left*), Pmax (*mid left*), Tmax (*top right*), Tmin (*mid right*) and the Pmin–Pmax differences (*lower left*) and Tmax–Tmin differences (*lower right*). The vectors indicate moisture transport **Q**, the vertical integral of q**v** in kg/(ms). Unit vector length is 200 kg/(ms), except for the lower right (Tmax–Tmin) where it is set to 30. Purple vectors indicate moisture transport larger than 300 kg/(ms) (*lower left*) or 50 kg/(ms) (lower right)

we do not see continued south-westerly/westerly winds or moisture transport reaching from the south-west coast of North Africa into Asia. This could be related to the relatively low resolution, and therefore reduced orography, in the models used by Prell and Kutzbach (1987) and Tuenter et al. (2003). Low resolution could also explain why the double precipitation peak over tropical North Africa during a precession maximum is not present in EC-Bilt (Tuenter et al. 2003), because in EC-Bilt the tropics consist of only a few grid boxes. The higher resolution of EC-Earth enables the model to respond better to the different annual cycle in insolation forcing within and outside of the tropics. Also, EC-Bilt shows a smaller precipitation response to the insolation forcing, of 101 and 8.9 % for precession and obliquity respectively (E. Tuenter pers.comm.), for insolation changes of 20.1 and 0.27 %, compared to 471 and 25.1 % for EC-Earth (0°N:30°N JJA). Whether the precipitation changes in north-westernmost Africa, the link to the low pressure centre over Asia and the double peak in precipitation in the Pmax experiment are related to the high resolution and/or sophisticated parametrizations remains to be tested in further sensitivity analyses.

Another notable difference with Tuenter et al. (2003) is that in their study increased moisture transport from

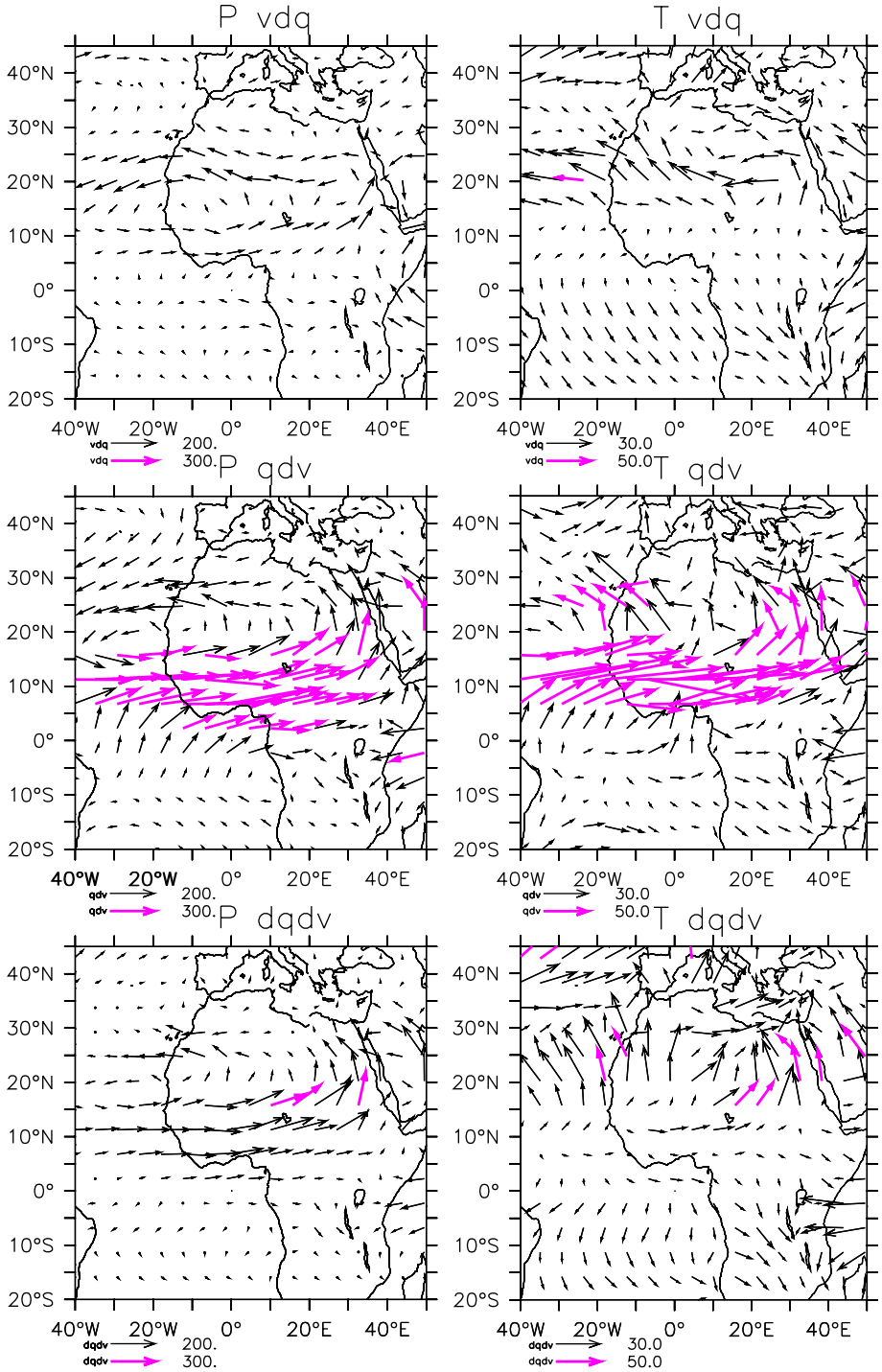

Fig. 11 June–July–August average changes in moisture transport terms (kg/(ms)). Changes due to humidity, with fixed winds, are given at the top ($\mathbf{v}\Delta q$). Changes due to wind, with fixed humidity, are given in the middle ($q\Delta\mathbf{v}$). Changes due to both wind and humidity are given at the bottom ($\Delta q\Delta\mathbf{v}$). All are vertically integrated. Unit vector length is 200 kg/(ms) (*black*) and 300 kg/(ms) (*purple*) on the left for precession, and 30 kg/(ms) (*black*) and 50 kg/(ms) (*purple*) on the right for obliquity (as in the lower part of Fig. 10)

the north plays an important role in bringing the precession and obliquity signals into the monsoon region. They used a quasi-geostrophic model that has very little transport of moisture and energy across the equator, which could explain the importance of remote high latitude forcing. It could also explain the smaller precipitation change in their study. In EC-Earth, increased transport from both the northern and southern tropical Atlantic dominates for both precession and obliquity and the precipitation change is larger. North of the monsoon region humidity changes are small and increased moisture transport from the north is much less important.

EC-Earth v2.2 lacks dynamic ice sheets, so the obliquity signal in the North African monsoon in our study does not originate from (high-latitude) glacial fluctuations, as is often assumed in the interpretation of paleoclimate records.

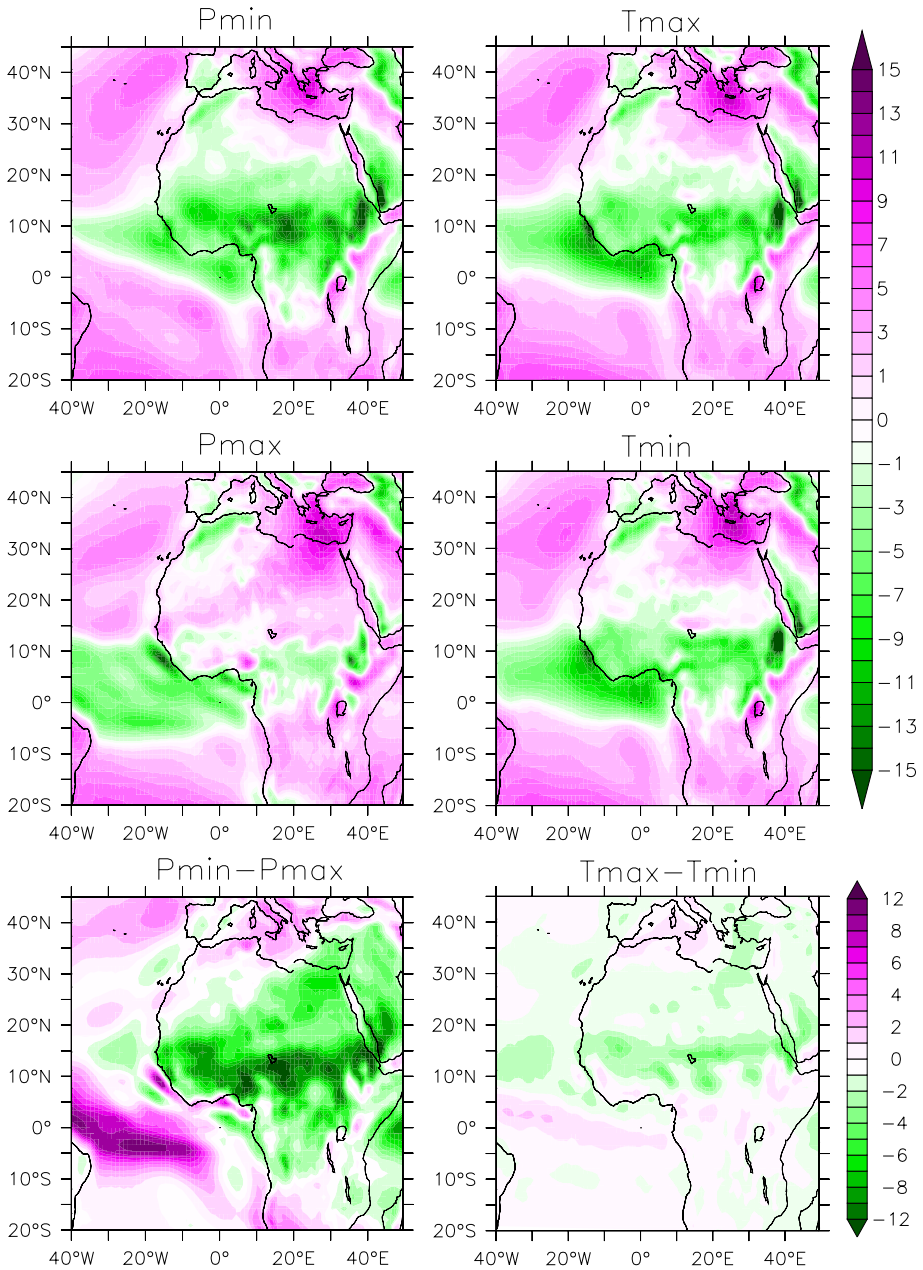

Fig. 12 June–July–August average vertical velocity at 500 hPa in 10^{-2} Pa/s in the Pmin experiment (*top left*), Pmax (*mid left*), Tmax (*top right*), Tmin (*mid right*) and the Pmin–Pmax differences (*lower left*) and Tmax–Tmin differences (*lower right*). *Green* indicates upward motion, *purple* indicates downward motion

Our findings imply a more direct response of tropical climate to obliquity changes, in agreement with studies that find only a short time lag with respect to obliquity and those that find obliquity signals in warm climate conditions (i.e. prior to ice age dominated climates of the past 3 Ma). A more detailed discussion on how obliquity influences low-latitude climate at all longitudes will be given in a separate paper.

An important component that is not yet included in the EC-Earth model, besides dynamic ice sheets, is dynamic vegetation, which could alter the monsoonal response to orbital forcing. Especially over the Sahel and the Sahara vegetation is likely to increase given the large orbital-induced precipitation enhancement (Fig. 3). Several Mid-Holocene studies show the positive feedbacks of a lower albedo (e.g. Ganopolski et al. 1998; Braconnot et al. 1999; Bonfils et al. 2001) as well as an increased sensible heat flux due to increased roughness length and an increased latent heat flux due to increased evapotranspiration (e.g. Texier et al. 2000; Levis et al. 2004). Thus, including vegetation would likely increase the monsoonal response to orbital forcing. Another point of improvement is that the experiments are relatively short (100 years), due to the model being computationally expensive and limitations in computing time. Longer runs might result in a more equilibrated climate, which becomes important when

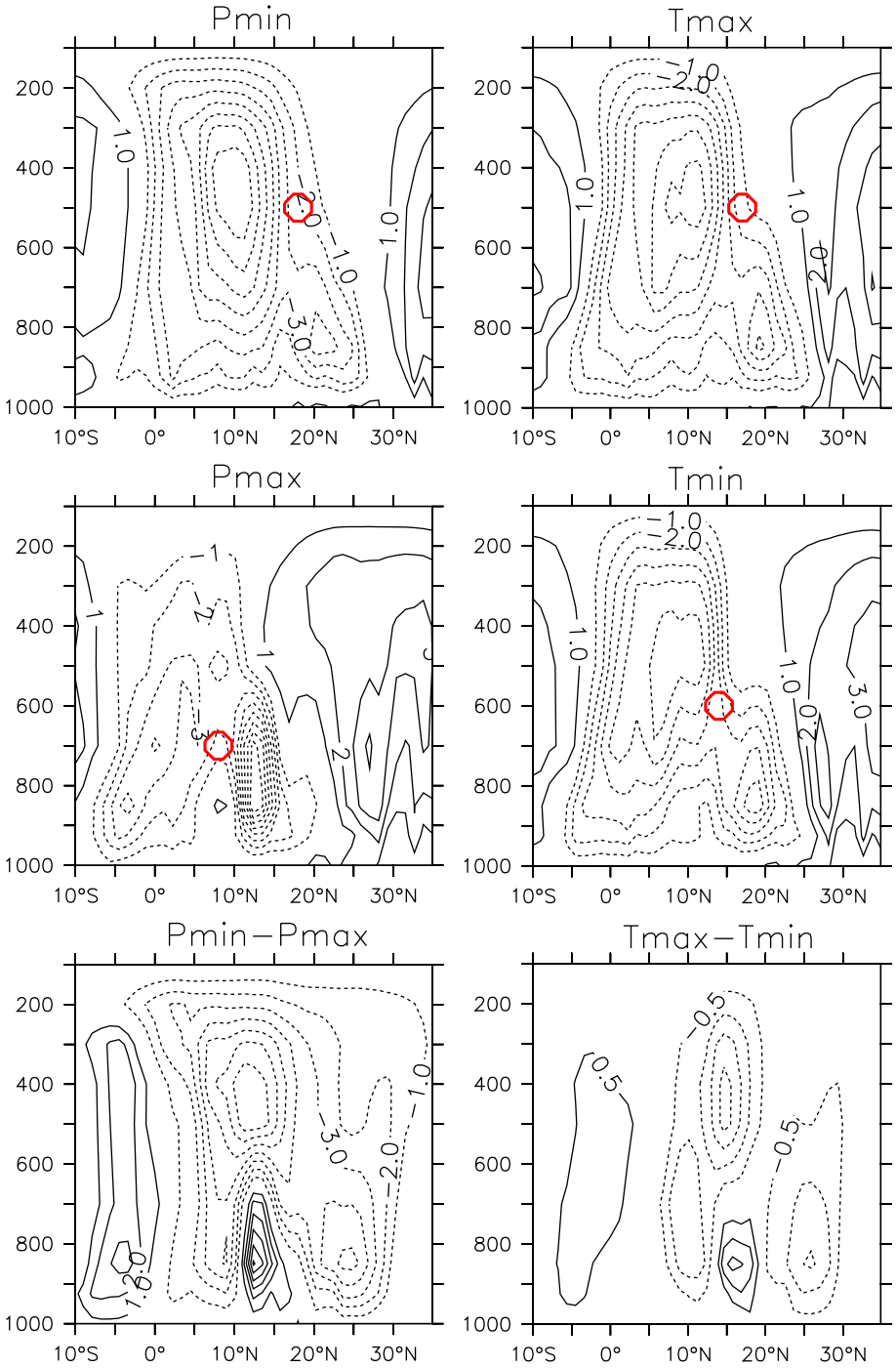

Fig. 13 June–July–August average vertical velocity hPa in 10^{-2} Pa/s averaged 30°W:40°E, in the Pmin experiment (*top left*), Pmax (*mid left*), Tmax (*top right*), Tmin (*mid right*) and the Pmin–Pmax differences (*lower left*) and Tmax–Tmin differences (*lower right*). *Contour* level is 1×10^{-2} Pa/s except for the lower right figure where it is 0.5×10^{-2} Pa/s. The *red circle* marks the location of the African Easterly Jet (AEJ), based on the location of maximum JJA 10°W:10°E easterly wind (Nicholson 2009)

studying climate components with longer response times, such as the deep ocean circulation. However, the atmospheric variables that we investigated in this study, especially precipitation, are sufficiently equilibrated.

Furthermore, although a full model-data comparison is beyond the aim of the present study, we note that model output such as presented here can be combined with extensive paleoclimate proxy data, such as marine records (e.g. Rossignol-Strick 1985; Pokras and Mix 1987; Larrasoaña et al. 2003; Ziegler et al. 2010), to improve our understanding of monsoon changes on orbital time scales. Continental records of lakes, fossil river channels and vegetation patterns over the Sahara also suggest a close link between orbitally-forced wet periods in the Sahara and the occupation, migration and evolution of hominins (e.g. Trauth et al. 2009; Drake et al. 2013; Larrasoaña et al. 2013). Such wet periods in the Sahara occurred at times of minimum precession and high eccentricity, similar to our Pmin case.

Also, fossil river channels suggest that at such times there were more routes of water transport to the Mediterranean besides the Nile (e.g. Osborne et al. 2008; Drake et al. 2011), affecting the Mediterranean Sea. The latter will be discussed in a future manuscript.

To conclude, we argue that both the precession and obliquity signals in the North African summer monsoon originate from enhanced moisture transport from the tropical Atlantic. The precession-induced changes are stronger, as the insolation change is much larger than the obliquity-induced change. Considering the near-zero obliquity-induced tropical insolation changes, we propose that the cross-equatorial insolation gradient may play an important role. We therefore disagree with the remote mid- to high-latitude forcing of Tuenter et al. (2003).

Acknowledgments Computing time was provided by the Royal Netherlands Meteorological Institute (KNMI) and the European Center for Medium-range Weather Forecast (ECMWF). Joyce Bosmans was funded by a "Focus en Massa" Grant of Utrecht University, the Netherlands. The authors thank the editor and two anonymous reviewers for their comments which helped improve this manuscript.

References

Balsamo G, Viterbo P, Beljaars A, van den Hurk B, Hirschi M, Betts AK, Scipal K (2009) A revised hydrology for the ECMWF model: verification from field site to terrestrial water storage and impact in the integrated forecast system. J Hydrometeorol 10:623–643. doi:10.1175/2008JHM1068.1

Bechtold PKM, Jung T, Doblas-Reyes F, Leutbecher M, Rodwell MJ, Vitart F, Balsamo G (2008) Advances in simulating atmospheric variability with the ECMWF model: from synoptic to decadal time-scales. Q J R Meteorol Soc 134:1337–1351. doi:10.1002/qj

Berger AL (1978) Long-term variations of daily insolation and quaternary climatic changes. J Atmos Sci 35:2362–2367

Bonfils C, de Noblet-Ducoudre N, Braconnot P, Joussaume S (2001) Hot Desert Albedo and climate change: Mid-Holocene monsoon in North Africa. J Clim 14:3724–3737

Bosmans JHC, Drijfhout SS, Tuenter E, Lourens LJ, Hilgen FJ, Weber SL (2012) Monsoonal response to Mid-Holocene orbital forcing in a high resolution GCM. Clim Past 8:723–740. doi:10.5194/cp-8-723-2012

Braconnot P, Joussaume S, Marti O, de Noblet N (1999) Synergistic feedbacks from ocean and vegetation on the African monsoon response to Mid-Holocene insolation. Geophys Res Lett 26(16):2481–2484

Braconnot P, Otto-Bliesner B, Harrison S, Joussaume S, Peterchmitt JY, Abe-Ouchi A, Crucifix M, Driesschaert E, Fichefet T, Hewitt CD, Kageyama M, Kitoh A, Laine A, Loutre MF, Marti O, Merkel U, Ramstein G, Valdes P, Weber SL, Yu Y, Zhao Y (2007) Results of PMIP2 coupled simulations of the Mid-Holocene and last glacial maximum—part 1: experiments and large-scale features. Clim Past 3(2):261–277

Braconnot P, Marzin C, Gregoire L, Mosquet E, Marti O (2008) Monsoon response to changes in Earth's orbital parameters: comparisons between simulations of the Eemian and of the Holocene. Clim Past 4(4):281–294

Chen GS, Zhengyu L, Clemens SC, Prell WL, Liu X (2011) Modeling the time-dependent response of the Asian summer monsoon to obliquity forcing in a coupled GCM: a PHASEMAP sensitivity experiment. Clim Dyn 36:695–710. doi:10.1007/s00382-010-0740-3

Clement A, Hall A, Broccoli A (2004) The importance of precessional signals in the tropical climate. Clim Dyn 22:327–341

de Noblet N, Braconnot P, Joussaume S, Masson V (1996) Sensitivity of simulated Asian and African summer monsoons to orbitally induced variations in insolation 126, 115 and 6 kBP. Clim Dyn 12:589–603

Drake NA, Blench RM, Armitage SJ, Bristow CS, White KH (2011) Ancient watercourses and biogeography of the Sahara explain the peopling of the desert. Proc Natl Acad Sci 108(2): 458–462. doi:10.1073/pnas.1012231108, http://www.pnas.org/content/108/2/458.full.pdf+html

Drake NA, Breeze P, Parker A (2013) Palaeoclimate in the Saharan and Arabian Deserts during the Middle Palaeolithic and the potential for hominin dispersals. Quatern Int 300:48–61

Erb MP, Broccoli AJ, Clement AC (2013) The contribution of radiative feedbacks to orbitally-driven climate change. J Clim. doi:10.1175/JCLI-D-12-00419.1

Ganopolski A, Kubatzki C, Claussen M, Brovkin V, Petoukhov V (1998) The influence of vegetation–atmosphere–ocean interaction on climate during the Mid-Holocene. Science 280(5371):1916–1919

Hazeleger W, Severijns C, Semmler T, Stefanescu S, Yang S, Wyser K, Wang X, Dutra E, Baldasano JM, Bintanja R, Bougeault P, Caballero R, Ekman AM, Christensen JH, van den Hurk B, Jimenez P, Jones C, Kallberg P, Koenigk T, McGrath R, Miranda P, van Noije T, Palmer T, Parodi JA, Schmith T, Selten F, Storelvmo T, Sterl A, Tapamo H, Vancoppenolle M, Viterbo P, Willen U (2010) EC-Earth: a seamless earth system prediction approach in action. Bull Am Meteorol Soc 91(10):1357–1363

Hazeleger W, Wang X, Severijns C, Stefanescu S, Bintanja R, Sterl A, Wyser K, Semmler T, Yang S, van den Hurk B, van Noije T, van der Linden E, van der Wiel K (2011) EC-Earth V2.2: description and validation of a new seamless earth system prediction model. Clim Dyn. doi:10.1007/s00382-011-1228-5

Joussaume S, Braconnot P (1997) Sensitivity of paleoclimate simulation results to season definitions. J Geophys Res 102(D2):1943–1956

Khon VC, Park W, Latif M, Mokhov II, Schneider B (2010) Response of the hydrological cycle to orbital and greenhouse gas forcing. Geophys Res Lett 37. doi:10.1029/2010GL044377

Kutzbach JE (1981) Monsoon climate of the early holocene: climate experiment with the earth's orbital parameters for 9000 years ago. Science 214(4516):59–61

Larrasoaña JC, Roberts AP, Rohling EJ, Winklhofer M, Wehausen R (2003) Three million years of monsoon variability over the northern Sahara. Clim Dyn 21:689–698. doi:10.1007/s00382-003-0355-z

Larrasoaña JC, Roberts AP, Rohling EJ (2013) Dynamics of green Sahara periods and their role in hominin evolution. PloS One 8(10):e76,514

Levis S, Bonan GB, Bonfils C (2004) Soil feedback drives the Mid-Holocene North African monsoon northward in fully coupled CCSM2 simulations with a dynamic vegetation model. Clim Dyn 23:791–802. doi:10.1007/s00382-004-0477-y

Lourens LJ, Antonarakou A, Hilgen FJ, Hoof AAMV, Zachariasse WJ (1996) Evaluation of the Plio–Pleistocene astronomical timescale. Paleoceanography 11(4):391–413

Lourens LJ, Wehausen R, Brumsack HJ (2001) Geological constraints on tidal dissipation and dynamical ellipticity of the Earth over the past three million years. Nature 409:1029–1034

Madec G (2008) NEMO ocean engine. Tech. rep., Institut Pierre-Simon Laplace, note du Pole de modelisation de l'Institut Pierre-Simon Laplace no. 27 (2008)

Mantsis DF, Clement B, Kirtman B, Broccoli AJ, Erb MP (2013) Precessional cycles and their influence on the North Pacific and North Atlantic summer anticyclones. J Clim. doi:10.1175/JCLI-D-12-00343.1

Merlis TM, Schneider T, Bordoni S, Eisenman I (2013a) Hadley circulation response to orbital precession. Part II: subtropical continent. J Clim 26. doi:10.1175/JCLI-D-12-00149.1

Merlis TM, Schneider T, Bordoni S, Eisenman I (2013b) The tropical precipitation response to orbital precession. J Clim 26. doi:10.1175/JCLI-D-12-00186.1

Montoya M, von Storch H, Crowley TJ (2000) Climate simulation for 125 kyr BP with a coupled ocean–atmosphere general circulation model. J Clim 13:1057–1072

Nicholson SE (2009) A revised picture of the structure of the monsoon and land ITCZ over West Africa. Clim Dyn 32:1155–1171. doi:10.1007/s00382-008-0514-3

Osborne AH, Vance D, Rohling EJ, Barton N, Rogerson M, Fello N (2008) A humid corridor across the Sahara for the migration of early modern humans out of Africa 120,000 years ago. Proc Natl Acad Sci 105(43):16444–16447. doi:10.1073/pnas.0804472105, http://www.pnas.org/content/105/43/16444.full.pdf+html

Pokras EM, Mix AC (1987) Earth's precessional cycle and Quaternary climatic change in tropical Africa. Nature 326:486–487

Prell WL, Kutzbach JE (1987) Monsoon variability over the past 150,000 years. J Geophys Res 92(D7):8411–8425

Rossignol-Strick M (1985) Mediterranean Quaternary sapropels, an immediate response of the African monsoon to variation of insolation. Palaeogeogr Palaeoclimatol Palaeoecol 49:237–263

Short DA, Mengel JG (1986) Tropical climatic phase lags and Earth's precession cycle. Nature 323:48–50

Sterl A, Bintanja R, Brodeau L, Gleeson E, Koenigk T, Schmith T, Semmler T, Severijns C, Wyser K, Yang S (2011) A look at the ocean in the EC-Earth climate model. Clim Dyn. doi:10.1007/s00382-011-1239-2

Texier D, de Noblet N, Braconnot P (2000) Sensitivity of the African and Asian monsoons to Mid-Holocene insolation and data-inferred surface changes. J Clim 13:164–181

Trauth MH, Larrasoaña JC, Mudelsee M (2009) Trends, rhythms and events in Plio–Pleistocene African climate. Quatern Sci Rev 28(5):399–411

Tuenter E, Weber SL, Hilgen FJ, Lourens LJ (2003) The response of the African summer monsoon to remote and local forcing due to precession and obliquity. Glob Planet Change 36:219–235. doi:10.1016/S0921-8181(02)00196-0

Valcke S, Morel T (2006) OASIS3 user guide. Tech. rep., CERFACS, prism technical report. http://www.prism.enes.org/Publications/Reports/oasis3_UserGuide_T3.pdf

van der Laan E, Gaboardi S, Hilgen FJ, Lourens LJ (2005) Regional climate and glacial control on high-resolution oxygen isotope records from Ain el Beida (latest Miocene, northwest Morocco): a cyclostratigraphic analysis in the depth and time domain. Paleoceanography 20:1–22. doi:10.1029/2003PA000995

Ziegler M, Tuenter E, Lourens L (2010) The precession phase of the boreal summer monsoon as viewed from the eastern Mediterranean (ODP Site 968). Quatern Sci Rev 29(11–12):1481–1490. doi:10.1016/j.quascirev.2010.03.011